Detecting In-Season Crop Nitrogen Stress of Corn for Field Trials Using UAV- and CubeSat-Based Multispectral Sensing

Yaping Cai , *Student Member, IEEE*, Kaiyu Guan , Emerson Nafziger,
Girish Chowdhary , *Senior Member, IEEE*,
Bin Peng, Zhenong Jin, Shaowen Wang , and Sibo Wang

Abstract—Nitrogen (N) fertilizer management is one of the main concerns for precision agriculture under corn production, which aims to not only maximize the profits, but also ensure environmental sustainability. Effective N fertilizer management can either avoid N stress or provide timely and accurate detection of in-season N stress for remedies. Traditional N trial experiments to evaluate different N management practices have to wait until harvest, and do not allow tracking of when and how N stress develops. Meanwhile, rapidly developed remote sensing technology offers new opportunities for in-season evaluation of N status and detection of N stress for crops, including both the unmanned aircraft vehicle (UAV)-based and satellite-based multispectral sensing. In this study, we collected weekly multispectral images of UAV and Planet Lab's CubeSat, as well as various other ground measurements for an experimental cornfield that included 28 N management treatments in Central Illinois, 2017. We found that both the UAV- and CubeSat-based multispectral sensors were able to detect N stress at vegetative stages before tasseling, and could detect changes in the level of N stress through derived chlorophyll index green (CIg) for different N management practices. The CubeSat-based CIg showed high consistency with the UAV-based CIg (correlation above 0.9), which indicated the potential of CubeSat-based CIg to be applied for N stress detection at a larger spatial scale. This study demonstrates that the UAV- and CubeSat-based multispectral sensing has the promising potential to monitor N stress of corn throughout the growing season, which may assist decision making of N management.

Index Terms—Corn nitrogen stress, CubeSat, in-season detection, Planet Lab, unmanned aerial vehicles (UAV).

I. INTRODUCTION

FERTILIZER management for modern agriculture aims to supply sufficient fertilizer amounts to avoid nutrient stress of crops and allow crops to realize their maximum yield potential [1]–[3]. Meanwhile, fertilizer management also aims to avoid overapplication to ensure environmental sustainability [4]–[6], as excessive fertilizer can escape from agroecosystems through volatilization, denitrification, leaching, and runoff, and cause environmental concerns [2]. In the US Corn Belt, which produces nearly 40% of global corn production, the relatively inexpensive N fertilizer compared with the undesirable consequence of underfertilization for crop yield motivates farmers to apply N in excess of demonstrated need, with the additional amount as "insurance" against yield penalty [3]. As a consequence, only one-third to half of the N fertilizer input is absorbed in the harvested product [7], [8], whereas substantial N stays in the soil may become a financial waste and create potential threats to the environment [9]–[11]. Optimizing fertilizer management practice and improving N use efficiency (NUE) are thus critical for agricultural production and environmental sustainability in the US Corn Belt.

Optimal fertilizer management has as its goal the provision of N to the crop using correct rate, type, timing, and application method of fertilizer. While variable rate technology is available for farmers to apply N with various amount to meet site-specific demand, the adoption rate is low, and the majority of farmers retain their tradition of flat rate application [12]–[15]. In that sense, timing and amount of N fertilizer are the two key factors in N management. Common practices in the US Corn Belt for fertilizer applications are that farmers/producers apply N fertilizer as one main application, mostly in spring and/or in the fall (with ammonia) where appropriate, and often some also applied in season [16]–[19]. These common applications may apply too much N either in fall or in spring, which would cause more N

Y. Cai and S. Wang are with the CyberGIS Center for Advanced Digital and Spatial Studies, Department of Geography and Geographic Information Science, University of Illinois at Urbana-Champaign, Urbana, IL 61801 USA (e-mail: cai25@illinois.edu; shaowen@illinois.edu).

K. Guan and B. Peng are with the College of Agricultural, Consumer and Environmental Sciences, and the National Center for Supercomputing Applications, University of Illinois at Urbana-Champaign, Urbana, IL 61801 USA (e-mail: kaiyug@illinois.edu; binpeng@illinois.edu).

E. Nafziger is with the Department of Crop Sciences, University of Illinois at Urbana-Champaign, Urbana, IL 61801 USA (e-mail: ednaf@illinois.edu).

G. Chowdhary is with the Department of Agricultural and Biological Engineering, University of Illinois Urbana-Champaign, Urbana, IL 61801 USA (e-mail: girishc@illinois.edu).

Z. Jin is with the Department of Bioproducts and Biosystems Engineering, University of Minnesota-Twin Cities, Saint Paul, MN 55108 USA (e-mail: jinzn@umn.edu).

S. Wang is with the Aspiring Universe Corporation, Champaign, IL 61820 USA (e-mail: sibo.wang@aspiringuniverse.com).

Color versions of one or more of the figures in this article are available online at http://ieeexplore.ieee.org.

Digital Object Identifier 10.1109/JSTARS.2019.2953489

leaching especially after heavy rainfall events, and may also lead to N deficiency for crops in the late growing season [13], [20]. All of the above may result in a low NUE. To improve the NUE, there are approaches suggesting to split the N application into multiple times (the so-called sidedressing) to synchronize crop N uptake and also reduce N leaching [21]–[23]. However, the key questions are not well answered about what amount and what time of N fertilizer should be applied. To address these questions, agronomists usually rely on farm trial plots to test different practices and compare end-of-season crop yield from different plots/practices.

Conventional evaluation for N trials has a critical challenge of having to wait till the end of the season to check harvested yield for different trials and different N management practices. This type of evaluation could not track when and how crop N stress is developed and progressed. Especially for split N applications, we require in-season tracking of crop condition to see when and how the N sidedressing may be needed to mitigate crop N stress in time to restore yield potential or not. Practically, if the N stress may be detected near real time, sidedressing decisions (when and how much to apply extra N fertilizer) can be optimized. Multiple approaches have been developed in the past to detect crop N stress, including visual inspection, tissue analysis, and using chlorophyll meter [24]. These existing approaches have a few obvious drawbacks [2], [24]–[27]. Primarily, these approaches are either empirical, labor intensive, or contain uncertainties by evaluating the whole field based on several samples that definitely leads to uncertainties. Better approaches to track in-season crop N stress are thus needed.

Recent rapid developments in both remote sensing technology and the unmanned aerial vehicle (UAV) offer new opportunities for real-time evaluation of N status and detection of N stress for crops. UAV systems allow practitioners to conduct real-time image data collections at local fields and at a high spatial resolution [25], [28]–[30]. Multispectral remote sensing technology provides useful reflectance information at different spectral bands (e.g., visible bands, red-edge bands, and near-infrared (NIR) bands) that are related to crop growing status and N contents [31]. For example, the collected multispectral data can be used to construct various vegetation indices (VI) to estimate crop N status, e.g., chlorophyll green index [32], chlorophyll red-edge index, and normalized differential red-edge index [26], [33]. Though the UAV-based multispectral sensing has been used for various applications in agricultural practice and particularly crop N stress [29], [34], [35], there are limited studies on using full growing-season data to trace N stress for further analyses like real-time N stress detection and to possibly infer N sidedressing decisions.

In the meantime, emerging CubeSat data have become available and can provide high spatiotemporal resolution, and various CubeSat-based applications have been proposed [36]–[38]. For example, Planet Lab has developed and maintained a complete PlanetScope constellation, which contains approximately 120 satellites that can image the world almost every day, and each PlanetScope satellite is a 3U CubeSat ($10 \times 10 \times 30$ cm, 1U represents 10 cm). PlanetScope images have a spatial resolution of ~ 3 m and contain four spectral bands (Blue, Green, Red,
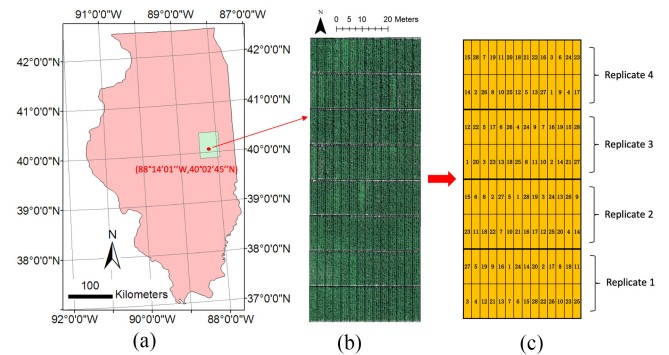

Fig. 1. Study area and the field trials. (a) Location of the experimental field. (b) UAV image on July 25th (91 DAP). (c) Field trials with treatment numbers in each plot.

and NIR), which has the potential to be used for monitoring subfield crop conditions. However, to the best of our knowledge, no existing work has been done yet to use CubeSat-based multispectral sensing for trial-plot in-season N-stress detection. It is important to investigate whether the CubeSat-based multispectral sensing has the potential for in-season N-stress detection at subfield scales, since it may have great potentials for large-scale applications of crop N stress monitoring.

In this study, we compared the UAV- and CubeSat-based multispectral images to study in-season corn crop N stress at a site in the 2017 growing season in Central Illinois. We focused on a comprehensive N-trial experiment, which included 28 N management practices varied by different amounts of N fertilizer, different ways to split N fertilizer, and different timing of sidedressing. We systematically evaluated the ability of using UAV- and CubeSat-based multispectral sensing to track crop growth conditions and N stress over the whole growing season for different N management practices. Our study aims to address the following research questions:

Question 1: How well can UAV- or CubeSat-based multispectral sensing capture N stress symptoms and its temporal development in corn?

Question 2: What are differences and similarities between UAV- and CubeSat-based multispectral sensing in terms of capturing the N stress of corn?

II. DATA AND METHODS

A. Study Area and Field Trials

The experimental site is located south of the University of Illinois at Champaign-Urbana, in Champaign County, Illinois [see Fig. 1(a)]. Champaign County is in the central U.S. Corn Belt region, where corn and soybeans are the predominant crops; corn and soybeans grow on $\sim 96\%$ of the cropland in Champaign County [39]. The area has a humid continental climate, with warm summers and cold, moderately snowy winters, which typically allows production of only one annual crop each year. During the growing season (May–September), the average temperature is $21.02 \pm 2.93\,°C$, and the accumulated precipitation is 533.15 mm (1981–2010 Climate Normals). As is common in this region, the experimental site was rainfed, without supplemental irrigation.

The field experiment included 28 different N management practices. A field about 0.5 ha in size was divided into eight ranges from North to South. Each range consisted of 14 side-by-side plots, with each plot consisting of four, 76-cm rows (3 m wide by 12.8 m long), with cross-alleys 0.9 m wide between ranges. Each replicate consisted of two ranges [see Fig. 1(c)]; there were four replicates of the experiment, laid out as a randomized complete-block design. The N management practices included a set of six N rates ranging from 0 to 250 lb/acre (0–280 kg/ha) applied as urea–ammonium nitrate (UAN) solution injected between rows at planting, and an additional 22 treatment combinations of application timing, N fertilizer form, and application method).

In this study, we focused on those management practices that most directly addressed our research questions; that is, how the different amounts and application timing of N fertilizer affect crop yield and can be captured by UAV- and CubeSat-based multispectral sensing. For this study, we focused on treatments within the following three groups of N management practices: we use "x–y N" hereafter to represent the N management practice with x lb/acre (1.12x kg/ha) planting-time application, and y lb/acre (1.12y kg/ha) sidedressing, and we also specify the growth stage for sidedressing by using "@ stage."

1) One-time application with different amounts: N rates applied as UAN solution injected between corn rows at planting: 0–0 N, 50–0 N, 100–0 N, 150–0 N, 200–0 N, and 250–0 N.
2) Two-time applications with different allocations of a fixed amount of N: injected UAN split between planting and sidedressing at stage V5–V6 (40 days after planting (DAP)) with a total of 150 lb/acre (168 kg/ha): 50–100 N, 0–150 N, and 100–50 N.
3) Two-time applications with different sidedressing timing, with 100 lb (45.4 kg) injected at planting and 50 lb (22.7 kg) sidedressed at different corn growth stages: 100–50 N @V5–6, 100–50 N @V9–10, and 100–50 N @VT. The VT application was made by dribbling the UAN near the row using a hand boom.

B. Data Collection and Preprocessing

We collected both remote sensing data and *in situ* measurements, with a total of seven types of data. Remote sensing data include UAV-based multispectral images and Planet Lab's CubeSat-based multispectral images. *In situ* measurements include leaf chlorophyll content data measured for the center of the top-canopy leaves, avoiding the leaf tip and base [40] and using a soil-plant analyses development (SPAD) 502 meter (Konica Minolta, Västra Frölunda, Sweden), leaf area index data (LAI) measured using a LAI 2000 (LI-COR, Lincoln, Nebraska USA), leaf-level N content from destructive sampling of the center of the top-canopy leaves, avoiding the leaf tip and base [40], measured using a Costech ECS 4010 CHNSO Analyzer (Costech, Valencia, California, USA), crop phenological stages, and crop grain yield data measured using a 2009 Almaco SPC40 combine (Almaco, Nevada, Iowa, USA). Fig. 2 shows the collection dates of these measurements.
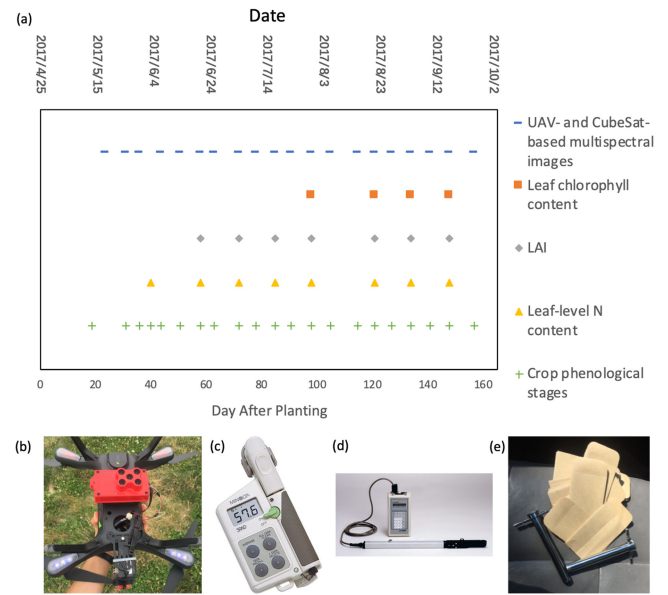

Fig. 2. Collection date of different data and the instruments used to collect the data. (a) *x*-axis represents date/DAP, and *y*-axis represents each specific data. The instruments on the bottom from left to right are (b) MicaSense Rededge mounted on 3DR Solo, (c) SPAD 502 meter, (d) LI-COR LAI 2000, and (e) punches and envelopes for leaf sampling.

1) Collection and Processing of the UAV-Based Multispectral Images: The UAV-based multispectral images were collected by the "RedEdge" sensor from MicaSense Company mounted on the UAV "3DR solo" from 3DR Company. The UAV was operated under Federal Aviation Regulation part 107 requirements. The UAV-based multispectral data contain five bands, including blue band (465–485 nm), green band (550–570 nm), red band (663–673 nm), red edge band (712–722 nm), and NIR band (820–860 nm). We calculated three VIs, i.e., normalized differential red edge (NDRE), chlorophyll index green (CIg), and chlorophyll index red-edge (CIre), which have been found to be closely related to canopy-level chlorophyll content [26], [32], [33]. The formulas of the three VIs are as follows:

$$\text{NDRE} = \frac{\text{NIR} - \text{red\_edge}}{\text{NIR} + \text{red\_edge}}$$

$$\text{CIg} = \frac{\text{NIR}}{\text{green}} - 1$$

$$\text{CIre} = \frac{\text{NIR}}{\text{red\_edge}} - 1. \tag{1}$$

The UAV-based multispectral data were collected weekly (slightly adjusted by 1–2 days earlier or later to make sure collection was conducted on clear sunny days) at noon (12:00–13:00 PM) and at 50 m height above ground with resolution of 3.5 cm/px. All the images were collected with 80% forward overlap and 60% side overlap to support the orthophoto images mosaicking processing. We then ingested all the raw images into the MicaSense DataHub image processing platform to generate orthophoto images. We further converted the raw collected image data in the form of digital number (DN) to reflectance following the instruction of Micasense [41].

2) Processing and Downscaling of Planet Lab's CubeSat Images: The CubeSat-based multispectral data, i.e., the daily PlanetScope images with 3.125-m spatial resolution, was downloaded from the Planet Lab's website (www.planet.com), which contains four bands, including blue band (455–515 nm), green band (500–590 nm), red band (590–670 nm), and NIR band (780–860 nm). Therefore, only CIg can be calculated from the PlanetScope images. The data are in the form of DN, which needs to be transformed into surface reflectance for further analysis. Due to cloud and revisit frequency issues, we lack the CubeSat-based images of specific dates when UAV images were collected. Therefore, we used the Landsat-MODIS fusion product (30-m resolution) based on the Satellite Data Integration [42] produced for Champaign county to perform a cumulative distribution function (CDF) correction for the Planet Lab's CubeSat data, and then conducted a pixelwise interpolation to fill invalid pixel (contaminated by clouds) to daily steps. Before the CDF, we also preprocessed the data for an "apparent atmospheric correction" and outlier detection. Specifically, we matched the mean and the standard deviation of the CubeSat data to the MODIS Nadir Bidirectional reflectance distribution function Adjusted Reflectance (NBAR) (MCD43) at the pixel level for the "apparent atmospheric correction," and we generated the invalid pixel mask by combining the unusable data mask provided by Planet Lab and the outlier pixels detected based on the difference time series of the CubeSat data and the MODIS NBAR.

The spatial resolution of the CubeSat data is 3.125 m, whereas the trial plot size is about 3 m∗13.5 m. Therefore, each pixel should contain information from multiple trial plots, and it is necessary to downscale the CubeSat data to get spectral information of each individual trial plot for the further plot-level analysis. Since the high-resolution UAV data contain detailed spatial information, we used it to further downscale CubeSat images to trial plot scales. The following linear model was used for downscaling:

$$T_i * \frac{\sum_{j=1}^{4} (X_{ij} * S_{ij})}{\sum_{j=1}^{4} S_{ij}} = Y_i$$

$$Y_{ij} = X_{ij} * T_i \ \ (j = 1, 2, 3, 4)$$

$$P_k = \sum_{i=1}^{m} (Y_{ik} * S_{ik}) \bigg/ \sum_{i=1}^{m} S_{ik}. \quad (2)$$

In the aforementioned equation, we suppose the pixel i contains information from plot j ($j = 1, 2, 3, 4$), shown in Fig. 3. X_{ij} ($j = 1, 2, 3, 4$) is the reflectance of a specific UAV-based band from plot j ($j = 1, 2, 3, 4$). S_{ij} is the area of plot j ($j = 1, 2, 3, 4$) within the pixel i. Y_i is the reflectance of a specific CubeSat-based band. T_i represents the linear relationship between UAV-based reflectance and CubeSat-based reflectance, which can be calculated from the equation. Y_{ij} is the CubeSat-based reflectance for part of the plot j from pixel i, which can be calculated by multiplying the T_i with X_{ij} ($j = 1, 2, 3, 4$). P_k is the final CubeSat-based reflectance for plot k ($k = 1, 2, 3, \ldots, 112$), which is the summation of the downscaling reflectance of plot k weighted by the area percentage. An example of the CIg spatial maps and time series for three distinctive plots is shown in Fig. 4
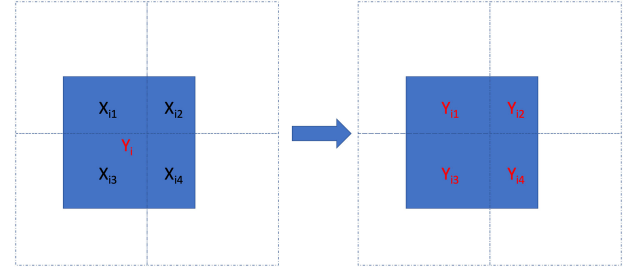

Fig. 3. Illustration of the downscaling method. Blue square represents pixel i of a specific CubeSat-based band with reflectance as Y_i, which overlaps with dashed-line square j ($j = 1, 2, 3, 4$) representing plot j ($j = 1, 2, 3, 4$). X_{ij} ($j = 1, 2, 3, 4$) is the reflectance of a specific UAV-based band from plot j ($j = 1, 2, 3, 4$). We want to calculate Y_{ij} ($j = 1, 2, 3, 4$) (the reflectance value of a specific CubeSat-based band) of pixel i within plot j ($j = 1, 2, 3, 4$).

for both UAV- and CubeSat-based images, which all show a clear seasonal cycle with a peak around 92 DAP.

3) Collection of In Situ Measurements: The *in situ* measurements were conducted to help interpret the remote sensing data and verify the resulting findings. Due to the labor intensiveness of the *in situ* measurements, only a part of the field was sampled, and the details are as follows.

Leaf-level N content data for specific plots were generated using the elemental analyzer on the leaf samples collected in the field bi-weekly. Nine plots within each of two replicates (Replicates 1 and 2 in Fig. 1) were selected: the six plots with planting-time applications of N rates ranging from 0 to 250 lb/acre (0–280 kg/ha) (i.e., 0–0 N, 50–0 N, 100–0 N, 150–0 N, 200–0 N, and 250–0 N); and three plots with planting-time applications and sidedressing at V5–V6 stage (i.e., 50–100 N, 0–150 N, and 100–50 N). We collected three leaf-punch samples (diameter of 1 cm) from center of the top-canopy leaves, avoiding the leaf tip and base [40]. Samples were dried and ground, and two subsamples were weighed, and wrapped in Al foil capsules for total N analysis.

Leaf-level chlorophyll content data were measured by SPAD-502. The SPAD measure has been used as an indicator of crop N status [24], [25], [27], [41], [43]. We took SPAD measurements for all the 28 plots within Replicate 1 (see Fig. 1), on top-canopy leaves on four plants (two measurements per plant) per plot biweekly. LAI was collected using LAI-2000 to evaluate the development of leaf area over time. We measured LAI on all 28 plots in Replicate 1 (see Fig. 1) at the biweekly intervals from 58 DAP to 148 DAP. Following the standard strategy [44], samples were evenly collected along the diagonal of each plot, including one measure above the canopy and four measures below the canopy with two repeats. Crop phenological stage information was collected every seven days by visual inspection. This information is used to identify the critical stages when evaluating *N* management based on the results from remote sensing. The plot-level yield data were collected through the yield sensor on the harvester, which serves as the standard metric for evaluating the effectiveness of different N management practices. All the remote sensing data and the field measurements are aggregated into plot level for further analysis by averaging the value within each plot.
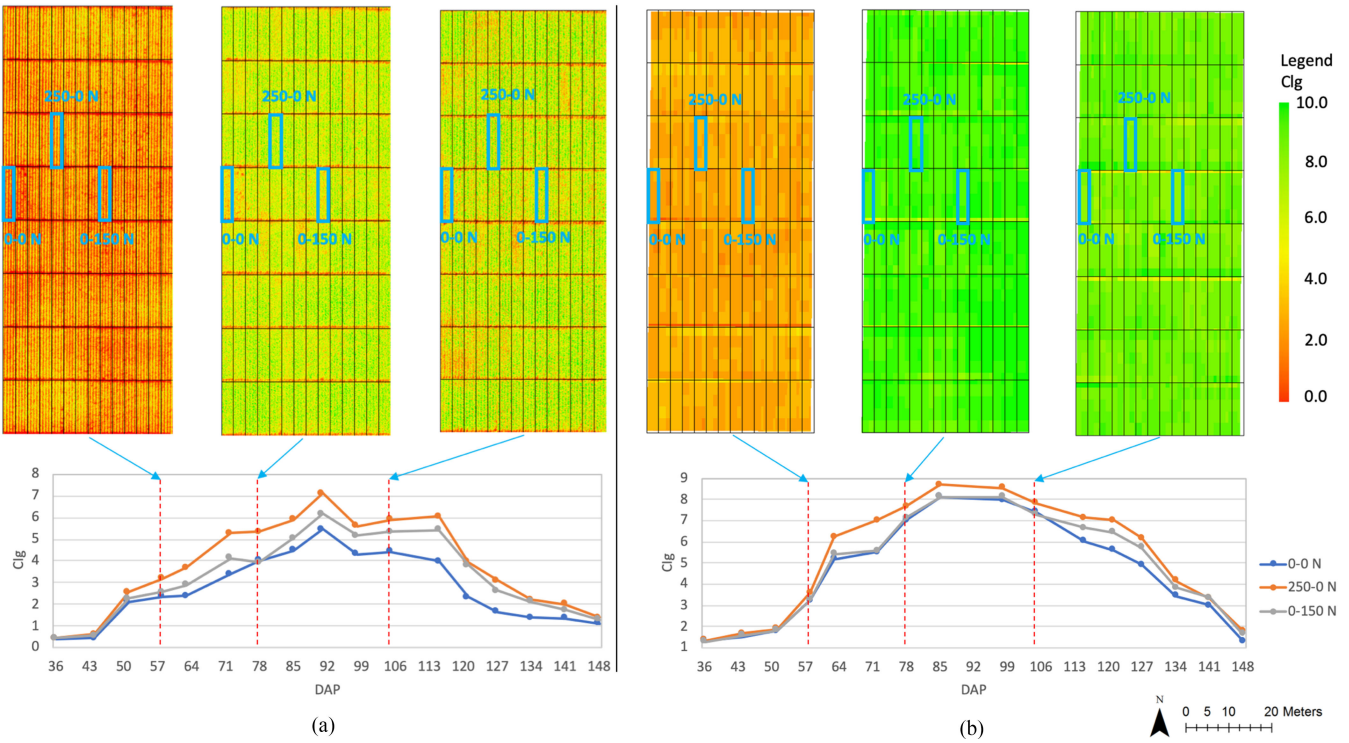
Fig. 4. Example of the CIg time series generated from (a) UAV- and (b) CubeSat-based multispectral sensing for three plots with three distinctive N management practices, i.e., 0–0 N, 250–0 N, and 0–150 N (the CubeSat-based CIg on 91 DAP is omitted due to the abnormal value). The top panels of both UAV- and CubeSat-based multispectral sensing show the CIg maps with three plots (highlighted with blue boundary) from three different stages, whose date is marked by blue arrows. The CubeSat-based CIg has higher values than UAV-based CIg.

C. Data Analysis

We correlated UAV-based VIs (i.e., CIg, CIre, and NDRE) or CubeSat-based CIg with various in-site measurements (e.g., LAI, leaf-level chlorophyll, leaf-level *N* content, and yield), and used the Pearson correlation coefficient (r) to quantify the capability of UAV-/CubeSat-based VIs in capturing the variability of those biophysical measurements. We then conducted three groups of analyses to answer the overarching questions raised in Section I.

1) Group #1 analysis focuses on one planting-time application but with different N rates amounts (50–0 N, 100–0 N, 150–0 N, 200–0 N, and 250–0 N). The analysis is benchmarked with the nonfertilized benchmark trial (0–0 N). The goal of this group analysis is to study the performance of UAV-/CubeSat-based VIs in detecting total N amount induced canopy difference.

2) Group #2 analysis compares the measurements from three sidedressing treatments at V5–6 stage, which have the same total N amount (150 lb/acre (168 kg/ha)) but different allocations to spring and sidedressing applications (0–150 N, 50–100 N, and 100–50 N). The comparison is benchmarked with the application practice of 150–0 N (i.e., apply 150 lb/acre (168 kg/ha) in spring and nothing afterwards). The goal of this group analysis is to study the performance of UAV-/CubeSat-based VIs in detecting the canopy difference induced by different sidedressing N amounts.

3) Group #3 analysis compares the measurements from the three sidedressing treatments with the same amounts in both spring and sidedressing applications (100–50 N) but different sidedressing application windows (V5-6, V9-10, and VT). The comparison is also benchmarked with the application practice of 150–0 N. The goal of this group analysis is to study the performance of UAV-/CubeSat-based VIs in detecting the canopy difference induced by different sidedressing time.

In all the three groups analyses, we tracked the individual trajectories of UAV-/CubeSat-based VIs, leaf-level *N* content, and their difference trajectories ($\triangle$VIs and $\triangle$N-content, $\triangle$CIg will be the focus of the $\triangle$VIs) between the treatments and the benchmark trials. Actual corn yield and yield differences between treatments and benchmark were also analyzed to reveal the yield benefits of different treatments. We note that the difference was calculated for all possible pairs of treatment and benchmark replicates (e.g., four replicates of treatment and four replicates of benchmark result in 16 pairs), and arithmetic mean as well as standard deviations were calculated from all the pairs.

Besides the three groups analyses, further correlation analyses were also conducted regarding the consistency between UAV-/CubeSat-based VIs to demonstrate the potential of CubeSat-based VIs to be applied at a large scale. To verify the consistency, first, we compared the UAV- and CubeSat-based VI across different plots and dates. Then, we compared the $\triangle$VI of UAV- and CubeSat calculated from the previous three groups analyses. Finally, we compared the time-series VI of UAV- and CubeSat
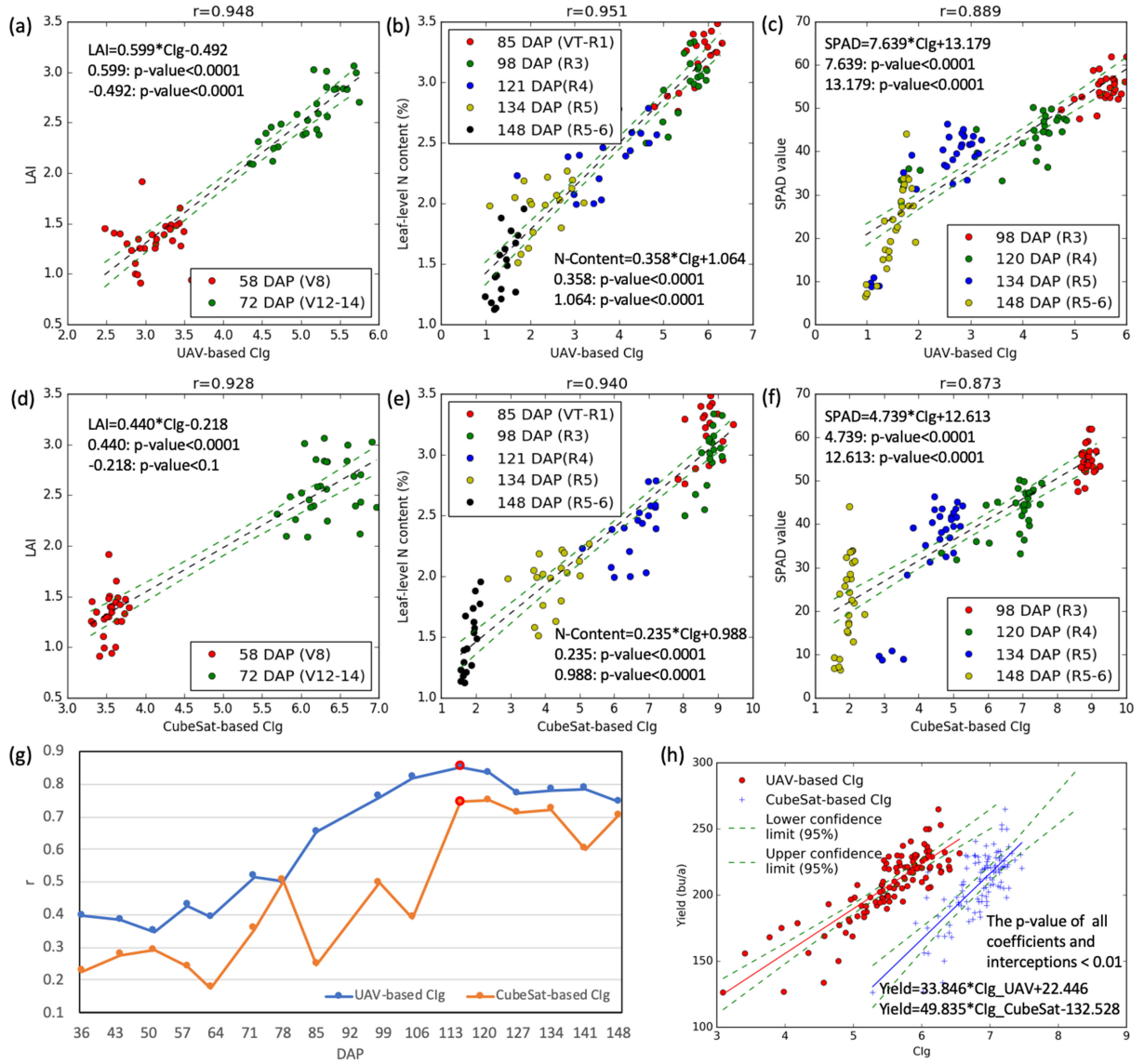
Fig. 5. Correlation between UAV-/CubeSat-based CIg and four biophysical measures, including LAI [m²/m², (a) and (d)], leaf-level N content [percentage in dry mass, (b) and (e)], SPAD value indicating leaf-level chlorophyll content [(c) and (f)], and yield [bu/a or 63 kg/ha, (g) and (h)]. (g) Correlation of CIg at different periods and end-of-season yield. (h) Linear regression on the date with the maximum correlation value in (g) (marked as red points). Different colors in (a)–(e) represent data collected on different DAP. The green dashed lines in (a)–(f) and (h) represent 95% confidence intervals of linear regression.

for each plot and generated a map showing the spatial pattern of the correlations.

III. RESULTS

A. Relationship Between VIs and Crop Biophysical Features

We found VI values to be highly correlated with different measured biophysical characteristics of the crop at different growing stages (see Figs. 5). UAV-based VIs showed highly positive correlations ($r > 0.915$) with LAI before tasseling [see Figs. 5(a)], which is consistent with the finding from Gitelson *et al.* (2003) and indicates UAV-based VIs can capture corn canopy development before tasseling. The correlation between UAV-based VIs and LAI after tasseling sharply decreased ($r < 0.636$), primarily due to canopy closing and senescence. We

also found UAV-based VIs had highly positive correlations with leaf-level *N* content after tasseling [see Figs. 5(b)] and leaf-level chlorophyll content during the sampling period [starting at the R3 stage; Figs. 5(c)]. Before tasseling, the leaf-level N content showed negative correlations with UAV-based VIs, which is consistent with previous findings [45], [46]. The CubeSat-based CIg showed similar correlation patterns with these biophysical measures as UAV-based CIg [see Fig. 5(d)–(f)].

Among different UAV-based VIs, we found UAV-based CIg has the best performance in terms of capturing plot-level variabilities of early season LAI ($r = 0.948$) and late season leaf-level N content ($r = 0.951$), whereas NDRE had a slightly better correlation with late season leaf-level chlorophyll ($r = 0.913$). Based on the performance of correlations with biophysical measures and the fact that only CIg can be calculated from
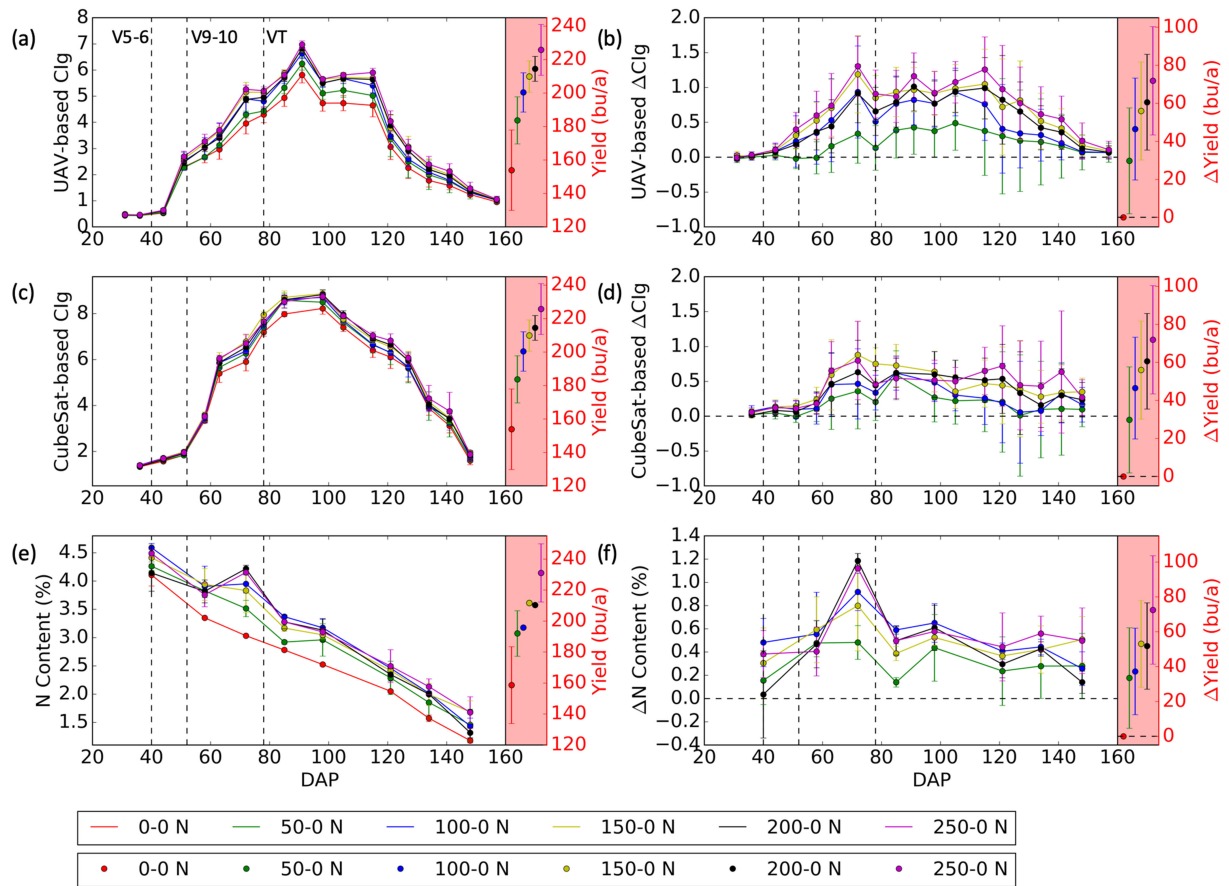
Fig. 6. Comparison of (a)–(d) UAV- and CubeSat-based CIg/△CIg, (e) and (f) leaf-level *N* content/△N-content, and yield/△yield (shaded area in (a)–(f)).The vertical dashed lines within each subfigure represent three phenology stages (V5–6, V9–10, and VT) of corn. (b), (d), and (f) Horizontal dashed lines mark the zero value of difference. The error bar represents the standard deviation calculated from the replicated trails. Note that yield/△yield values in (a)–(d) are based on all four replicates, while those in (e) and (f) are based on only two replicates. Some error bars in (e) are too short to be visible.

CubeSat-based multispectral sensing, we decided to use CIg in our following analysis.

The correlation between CIg and crop grain yield had a seasonal pattern, which increased in the vegetative and reproductive stages till ∼R3 stage and then decreased [see Fig. 5(g)]. CIg measures from UAV and CubeSat showed similar patterns of the above relationship, except that the CIg:yield correlation from UAV showed more gradual changes and higher values than that of CubeSat-based images. Further, the linear regression results of the date with the maximum correlation [highlighted red points in Fig. 5(g)] are shown in Fig. 5(h). The maximum value occurred at the middle of the reproductive stage instead of the late-vegetative/early-reproductive stage when the peak CIg occurred, highlighting the importance of late-season canopy N (as indicated from CIg).

B. Group #1 Analysis: Sensing the Impacts of Different N Fertilizer Amounts in One-Time Application

We focused on one planting-time application and looked at CIg responses from different trials with different N fertilizer amounts in this section, and find the UAV- and CubeSat-based multispectral sensing can detect N stress at an early stage (see

Fig. 6). In general, both UAV- and CubeSat-based CIg of different N treatments showed a similar seasonal cycle [see Fig. 6(a) and (c)], with a seasonal peak around 90 DAP (10 days after tasseling at the reproductive stage). More N fertilizer leads to higher CIg, which is further highlighted by the pattern of △CIg [see Fig. 6(b) and (d)]. Specifically, UAV-based △CIg gradually increased till the peak value around 70 DAP (closely before tasseling); it then remained relatively stable in the middle of the growing season (80–120 DAP), and drops continuously during the late growing season. CubeSat-based △CIg follows similar patterns but contained more noise at the late growing season.

UAV-based △CIg revealed information of in-season crop N stress [see Fig. 6(d)]. The UAV-based △CIg of 100–0 N was close to that of 200–0 N before senescence starts (∼120 DAP), and then matched well with that of 50–0 N during the senescence period. In comparison, the UAV-based △CIg of 150–0 N showed similar patterns with those of 200–0 N and 250–0 N throughout the growing season. Therefore, 100–0 N may not cause much N stress at the early and peak growing season, but ended up with N stress at the late growing season. Considering 150 lb/acre (168 kg/ha) of N may be a safe amount to guarantee the corn not experiencing N stress, we fixed the total amount of N fertilizer as 150 lb/acre (168 kg/ha) for the following two analyses which focus on sensing the impact of sidedressing (Section III-C
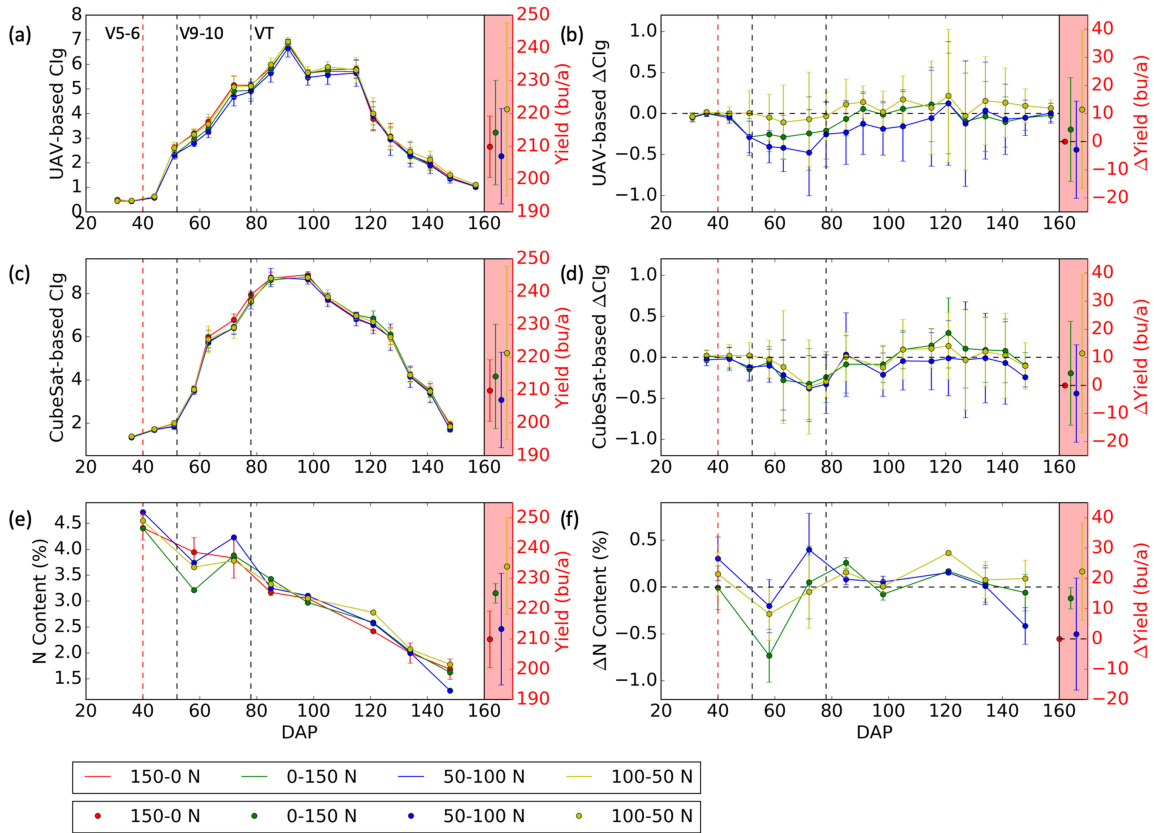
Fig. 7. Comparison of (a)–(d) UAV- and CubeSat-based CIg/△CIg, (e) and (f) leaf-level N content/△N-content, and yield/△yield (shaded area in (a)–(f)). The vertical dashed lines within each subfigure represent three phenology stages (V5–6, V9–10, and VT) of corn. The red vertical dashed line indicates the timing of sidedressing (around V5–6). (b), (d), and (f) Horizontal dashed lines mark the zero value of difference. The error bar represents the standard deviation calculated from the replicated trails. Note that yield/△yield values in (a)–(d) are based on all four replicates, while those in (e) and (f) are based on only two replicates. Some error bars in (e) are too short to be visible.

and III-D). Although the uncertainty of UAV-based △CIg could be largely due to the small sample size (only four replicates in this study), UAV-based △CIg of all the pairs around 60–70 DAP was significant (error bars above zero) except for 50–0 N, indicating N stress can be detected at an early stage through the UAV- and CubeSat-based multispectral sensing.

Leaf-level N content showed a decreasing trend from the beginning to the end of the growing season [see Fig. 6(e)], which is consistent with previous findings (Ata-Ul-Karim *et al.*, 2016; Reich *et al.*, 1997; Vos *et al.*, 2005). The seasonal patterns of leaf-level N content and CIg were thus significantly different. This may be largely due to the N dilution effect [46] as the growth rate of crop is faster than that of *N* taken. In addition, leaf-level *N* was measured on single leaves in the upper canopy, whereas multispectral CIg was a canopy measure that integrates leaf and canopy structure information [47]–[49]. Distinguishing the contributions from different levels of leaves and stems [50] may rely on the radiative transfer models [51], [52], which is beyond the scope of this research. However, the leaf-level △N-content showed a similar seasonal pattern as △CIg with seasonal peak around 70 DAP [see Fig. 6(f)]. The yield kept increasing when more N fertilizer is applied (shaded area in Fig. 6) at rates up to about 150 lb/acre (168 kg/ha), which was similar to the responses of CIg to *N* rate.

C. Group #2 Analysis: Sensing the Impacts of N Fertilizer Sidedressing

We compared measurements from the three sidedressing treatments (i.e., 0–150 N, 50–100 N, 100–50 N), taking the single planting-time application of 150–0 N as reference, and found that the UAV- and CubeSat-based CIg can track the progress of N stress development from these treatments (see Fig. 7). Both UAV- and CubeSat-based CIg [see Fig. 7(a) and (c)] showed a similar seasonal cycle as is shown in Fig. 6. However, either UAV- or CubeSat-based CIg representing different treatments cannot be distinguished from each other. In comparison, UAV-based △CIg [see Fig. 7(b)] not only distinguished different treatments, but also showed the time when the N stress occurred, intensified, or disappeared. For example, 50–100 N showed negative UAV-based △CIg at the early growing season caused by limited amount of planting-time application, which was consistent with the findings in Section III-B (i.e., 50 lb/acre (56 kg/ha) causes N stress). After sidedressing, UAV-based △CIg of 50–100 N continues to expand till 70 DAP and then reduced steadily, which indicates N stress is gradually alleviated with sidedressing. A similar pattern was found in 0–150 N except reduction of UAV-based △CIg started earlier, perhaps due to the larger amount of N sidedressing. The 100–50 N treatment showed small UAV-based △CIg at the early growing season,
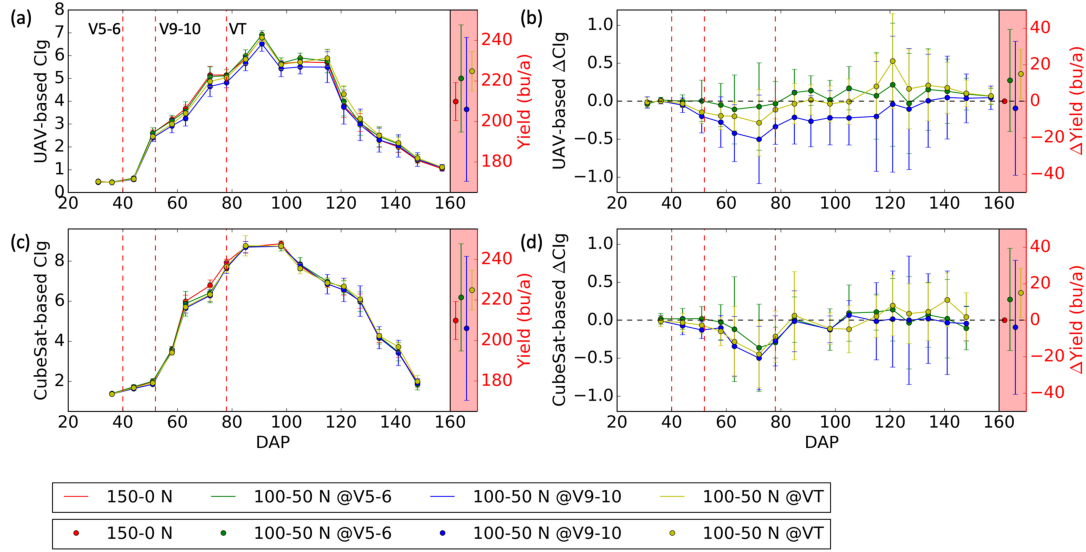
Fig. 8. Comparison of UAV- and CubeSat-based CIg/△CIg and yield/△yield (shaded area) for sidedressing at different stages. The vertical dashed lines within each subfigure represent three phenology stages (V5–6, V9–10, and VT) applied with sidedressing. (b) and (d) Horizontal dashed lines mark the zero value of difference. The error bar represents the standard deviation calculated from the replicated trails.

which is consistent with the findings in Section III-B (i.e., 100 lb/acre (112 kg/ha) causes limited/no N stress at the early growing stage). After sidedressing, UAV-based △CIg of 100–50 N becomes positive during rest of the growing season, indicating benefits gained from sidedressing. The CubeSat-based △CIg [see Fig. 7(d)] shows similar patterns as UAV-based △CIg with seasonal peak around 70 DAP, except that it fails to distinguish different treatments before 80 DAP.

An interesting finding was that there was a lag between △CIg and leaf-level △N-content after sidedressing, e.g., leaf-level △N-content has reduced around 70 DAP, whereas △CIg kept intensifying [see Fig. 7(b), (d), and (f)]. One possible explanation for this lag is that it takes time for crop to transform available N to chlorophyll content (e.g., CIg), which can be detected by remote sensing. The treatments (i.e., 0–150 N and 50–100 N) with limited planting-time N application show almost no difference in terms of △yield (≤5 bu/acre, shaded area in Fig. 7), whereas the treatment (i.e., 100–50 N) with abundant planting-time N application shows the benefits regarding the significant positive △yield (>10 bu/acre, shaded area in Fig. 7).

D. Group #3 Analysis: Sensing the Impacts of Different Timing in Sidedressing

We explored the timing impacts of sidedressing, and found the UAV- and CubeSat-based CIg can track the N stress development throughout the growing season for different N managements. Again, both UAV- and CubeSat-based CIg from different trials [see Fig. 8(a) and (c)] showed a similar seasonal cycle, and △CIg of both platforms had a seasonal peak around 70 DAP, which were all consistent with the results shown in Figs. 6 and 7. Among the three trials, sidedressing at V5-6 benefits the corn growth through reducing the time period of N stress, supported by its smaller negative △CIg around 70 DAP than other two treatments. Although being affected by the longest N stress in the early growing season, sidedressing at the critical

VT stage satisfies the N demand for reproductive development and leads to higher positive △CIg at the late growing season (after 110 DAP) as well as highest yield boost [see Fig. 9(b)]. For sidedressing at V9-10, we would suppose that its △CIg should be between the △CIg values with sidedressing at V5-6 and VT. That was not the case: △CIg from V9-10 sidedressing showed its abnormal negative value throughout the growing season, indicating that N stress was not alleviated. We found a possible explanation for such unexpected results. There was a strong precipitation one day before the N application @V9-10, which led to increased wetness in the soil. Then, the additional two days' precipitation following the N application tended flush downward, leading to the N lose through runoff and leaching. There was no precipitation after V5-6 within nine days, whereas there was very limited precipitation within six days after VT.

E. Consistency Between UAV- and CubeSat-Based CIg

To demonstrate the potential of CubeSat-based CIg to be applied at large scale, we conducted three correlation analyses for UAV- and CubeSat-based CIg regarding their consistency (see Fig. 9). The high correlation between UAV- and CubeSat-based CIg (0.91) across different plots and dates in Fig. 9(a) confirms the high consistency, though bias still exists. The correlation of UAV- and CubeSat-based △CIg [see Fig. 9(b)] that we used to compare different N management practices also showed a high value (0.89), and the spatial pattern of the correlation at the plot level was above 0.85 [see Fig. 9(c)], which all confirm their consistency.

IV. DISCUSSION

A. In-Season Crop N Stress Detection and Monitoring

Our results demonstrate the potential ability to use UAV- and CubeSat-based multispectral sensing to detect in-season crop N stress, and to monitor when the N stress is intensified, alleviated,
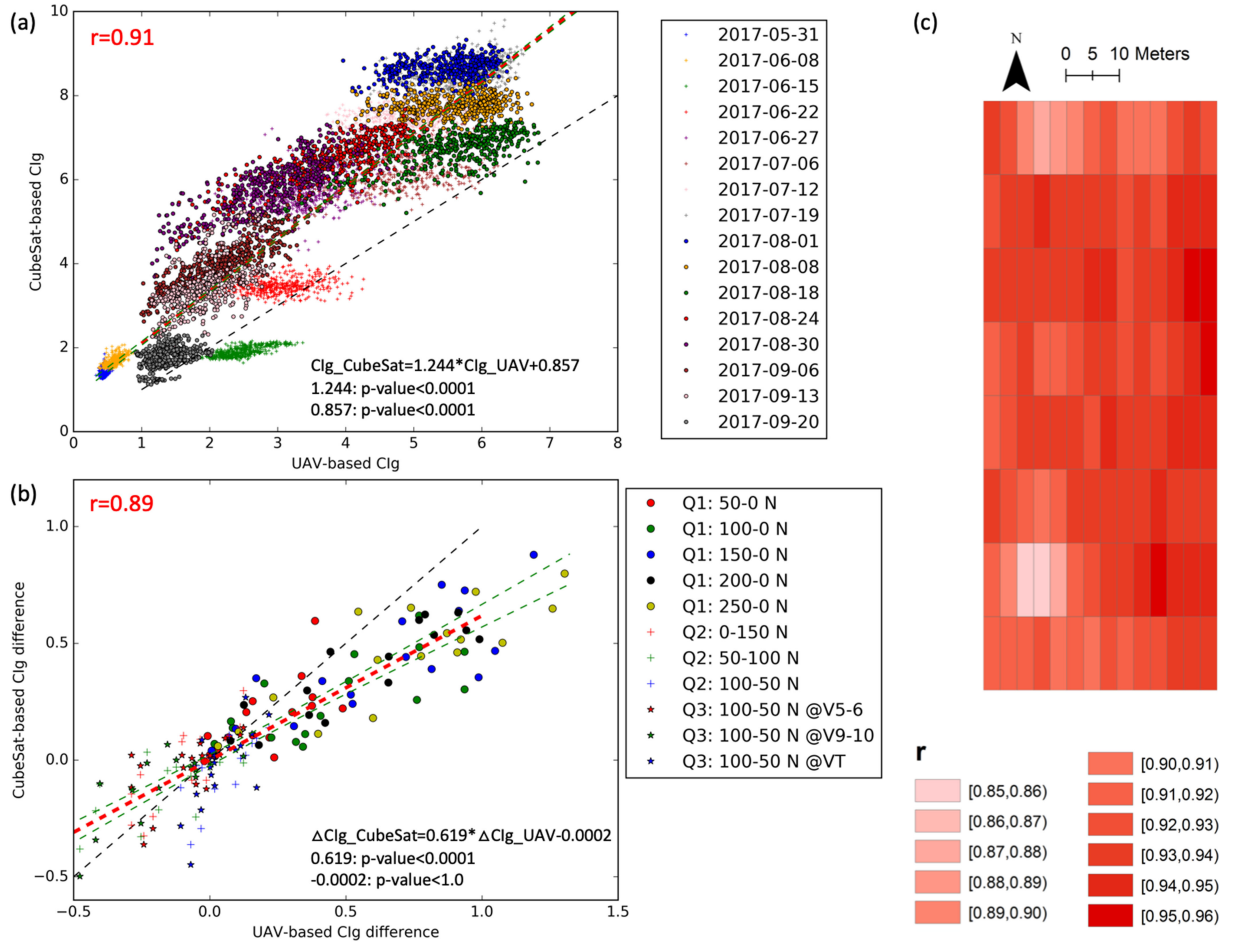
Fig. 9. Comparison between UAV- and CubeSat-based CIg. (a) Correlation between UAV- and CubeSat-based CIg. The points are marked with different styles to distinguish different dates. (b) Correlation between UAV- and CubeSat-based $\triangle$CIg from previous three analyses. The points are marked with different styles to distinguish different N treatments. In (a) and (b), the black lines represent the 1:1 line, the red lines are the fitted lines from linear regression, and the green-dashed lines represent 95% confidence intervals of the linear regression. (c) Spatial correlation map of UAV- and CubeSat-based CIg. The correlation of each plot is calculated using the time series of UAV- and CubeSat-based CIg.

or disappeared. At our site, the gradually intensified $\triangle$CIg till 70 DAP caused by the insufficient planting-time application (see Figs. 6–8) indicates the ability of UAV- and CubeSat-based CIg to detect N stress at the early stage (before tasseling). Based on the correlation analysis between VIs and the crop biophysical features in Section III-A, we attribute $\triangle$CIg to the difference in LAI [32], [33], [53], which means that the insufficient N fertilizer amount at an early stage may influence the canopy development of the crop. Our results also demonstrate that the UAV- and CubeSat-based CIg can monitor and track the N stress throughout the growing season, including when N stress is alleviated and even eliminated from sidedressing. For example, 0–150 N in Fig. 7 shows the $\triangle$CIg gradually decreases during the 70–100 DAP for treatments with sidedressing, indicating the crop with N stress may catch up with the unstressed crop by canopy development, generate more chlorophyll in leaves, or both during this period according to our previous correlation analysis. Another example is 100–50 N @VT in Fig. 8, which shows the $\triangle$CIg decreases to zero or even becomes positive value in the late growing season, which stands for more N/chlorophyll content in the leaves since the canopy stop developing during this period [32]. The leaf-level measures of N content confirm the results

derived from CIg. Even though the trends of CIg and N content are different, the trends of $\triangle$CIg and $\triangle$N-content are similar except there is a lag ($\sim$two weeks) when sidedressing was adopted (see Fig. 7), which should be considered when using UAV-/CubeSat-based CIg to track the crop status after remedy action is conducted in real world application.

B. Comparison Between UAV- and CubeSat-Based Multispectral Sensing

One goal of this study is to investigate whether the UAV- and CubeSat-based multispectral sensing have similar or varying performance in capturing the crop N stress. Our results show that the CubeSat-based CIg can achieve a similar performance in detecting in-season N stress as the UAV-based measures. The high consistency between UAV- and CubeSat-based CIg (see Fig. 9) indicates potentials of CubeSat-based multispectral sensing to be applied for crop N stress detection at larger spatial scales. More spatial details have been revealed from the measurements of UAV than CubeSat, which is largely expected due to the UAV's high spatial resolution and may also be the reason that the UAV-based CIg has higher correlation with the

final yield then CubeSat-based throughout the growing season [see Fig. 5(g)]. However, this may be much less a concern for row crops, as CubeSat's 3.125 m resolution usually is sufficiently fine to capture subfield spatial heterogeneity. For future trial-plot design, the size of the trial plot should be at least 6.25 (3.125∗2) m to have one pure pixel within the plot.

Both the UAV- and CubeSat-based multispectral sensing have their own pros and cons. For UAV-based multispectral sensing, it has high spatial resolution, flexibility to operate at anytime when weather allows, and extensibility to mount different sensors for different purposes. However, it is both time consuming and labor intensive (a pilot is needed based on the UAV regulation in the US) and requires relatively intensive data preprocessing. Recently, the network-connected UAVs allow the UAV swarm to cooperate for big tasks [54], [55], which may be a potential for the large area application in agriculture. However, such technology is not mature yet and its cost efficiency is still to be justified for practical applications. On the contrary, using some mature data processing pipelines for data correction mentioned in Section II-B2, the CubeSat-based multispectral sensing provides ready-to-use data that can be easily expanded to a large area. Over the past decades, the CubeSat constellation developed rapidly in the space industry and will provide higher spatiotemporal resolution images in the future [56].

C. Evaluations of N Management Practices

The ultimate goal for this study is to find the optimal N fertilizer management. Our study reveals the following findings with the further help of UAV- and CubeSat-based multispectral sensing besides the final yield. Meanwhile, since the following findings are based on one-year's trial experiments, we also suggest these findings with caution, and multiple-years trial or process-based modeling are further needed to corroborate these findings.

First, we find that higher rate of one planting-time application usually leads to more yield but with reduced marginal benefits, which is supported by the CIg time series that higher N has higher CIg throughout the growing season (see Fig. 6). This is consistent with the real-world N management practice that farmers tend to apply more N fertilizer to guarantee their final yield facing the interannual variation in weather; however, the decreased yield boost indicates the inefficiency. Second, with a fixed total amount of N fertilizer, we find the N sidedressing has equivalent or better performance comparing to the one planting-time application at our site (see Figs. 7 and 8). Both the allocation and the timing of the sidedressing affect the final yield. For our side, the first application with 100 lb/acre (112 kg/ha) provides enough N amount that leads to no N stress or recoverable N stress during the early stage, then the sidedressing at the critical stage when corn still has a large *N* demand (e.g., VT stage) seems to lead to better synchronization of plant N need. However, the weather condition, especially precipitation, should be considered for the real-world applications due to its roles in removing available inorganic N through runoff and

leaching; for example, the consecutive precipitations following the sidedressing at V9–10 stage have may affected performance of that N management practice (see Fig. 8).

D. Opportunity and Future Work

In this article, we have demonstrated the potential of using CubeSat-based CIg for the scaling up through the consistency between UAV- and CubeSat-based CIg (see Fig. 9). These findings indicate promising potential for using CubeSat data to track N stress at large scales. However, the real-world situation is more complicated when scaling up to large areas that need more considerations. First, the practical strategy may require farmers to apply sufficient N fertilizer to a certain area as the benchmark group [25], [31], [33]. Second, when the field scale is large, environmental factors (e.g., soil type, topography, etc.) may create significant spatial heterogeneity for the demand of N fertilizer. Thus, multiple benchmark groups with abundant N fertilizer under different situations may be needed, and how to design trial strategy and benchmark groups is a remaining and urgent question to be addressed. Third, different crop types may have distinctive responses (e.g., time and amount) when suffering N stress, which leads to different changes of VI [26], [53], [57]. Therefore, it is essential to treat different crop types separately, which requires spatial explicitly early-season crop type classification [58]. Finally, the UAV-based remote sensing may serve as the ground truth for the CubeSat-based remote sensing at a large scale application; however, how the UAV-based remote sensing is affected by sun azimuth angle, row orientation to incident light, etc., should be taken into account.

Another goal of this article is to compare the performance of different VIs (with and without red edge) with regard to their ability to track the N stress of crop. Even though the correlations between different UAV-based VIs and various biophysical measures were similar for our site, they may change for different fields, different crops, or different years [26], [33], [59]. More research is needed to explore the performance of different satellite-based VIs at a large scale. In addition, it is also difficult to generalize very much using data from a single trial. For example, the intensive precipitation may lead to the abnormal performance of 100–50 N @V9-10 (see Fig. 8).

V. CONCLUSION

In this study, we systematically evaluated the ability to use UAV- and CubeSat-based multispectral images to track crop growth conditions and N stress over the whole growing season for different N management practices at a research site in Central Illinois. We were able to show that CIg derived from both the UAV- and CubeSat-based multispectral images could track the appearance, intensification, and disappearance of crop N stress as measured by plant-based measurements. Specifically, our study shows that N stress occurs and intensifies before the corn tasseling stage at our experimental site, which allows enough time window to detect the stress and take remedy operations (i.e., sidedressing). The early N stress can be alleviated or even disappear afterward with the sidedressing. The UAV-based

CIg reveals more spatial details among different N treatments than CubeSat-based CIg at the plot level; however, the high consistency between UAV- and CubeSat-based CIg indicates the potential of CubeSat-based CIg to be applied at a larger scale. Both the CIg time series and final yield showed that N management practices with sufficient N fertilizer caused little or no N stress at early growth stages, and sidedressing at VT in this environment outperformed a single, planting-time application. This study demonstrates the UAV- and CubeSat-based multispectral sensing have the promising potential to monitor N stress of corn throughout the growing season. This method may not only be used to evaluate the N management practices, but also may have application in making N management decisions in fields.
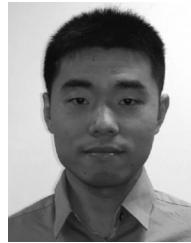
REFERENCES

[1] J. J. Meisinger, J. S. Schepers, and W. R. Raun, "Crop nitrogen requirement and fertilization," in *Nitrogen in Agricultural Systems*, (Agronomy Monographs 49). Madison, WI, USA: ASA Architectural Des., 2008, pp. 563–612.

[2] T. F. Morris *et al.*, "Strengths and limitations of nitrogen rate recommendations for corn and opportunities for improvement," *Agron. J.*, vol. 110, no. 1, pp. 1–37, Sep. 2018.

[3] P. C. Scharf, "Managing nitrogen," in *Managing Nitrogen in Crop Production*. Madison, WI, USA: Amer. Soc. Agronomy, Inc., 2015, pp. 25–76.

[4] F. J. Stevenson and D. R. Keeney, "Nitrogen management for maximum efficiency and minimum pollution," in *Nitrogen in Agricultural Soils*. Madison, WI, USA: Amer. Soc. Agronomy, Inc., 1982, pp. 605–649.

[5] S. Daberkow, M. Ribaudo, and O. Doering, "Economic implications of public policies to change agricultural nitrogen use and management," in *Nitrogen in Agricultural Systems*, (Agronomy Monographs 49). Madison, WI, USA: ASA Architectural Des., 2008, pp. 883–910.

[6] G. W. Randall, J. A. Delgado, J. S. Schepers, J. S. Schepers, and W. R. Raun, "Nitrogen management to protect water resources," in *Nitrogen in Agricultural Systems*. Madison, WI, USA: Amer. Soc. Agronomy, Inc., 2008, pp. 911–945.

[7] X. Zhang, E. A. Davidson, D. L. Mauzerall, T. D. Searchinger, P. Dumas, and Y. Shen, "Managing nitrogen for sustainable development," *Nature*, vol. 528, no. 7580, pp. 51–59, Nov. 2015.

[8] K. G. Cassman, A. Dobermann, and D. T. Walters, "Agroecosystems, nitrogen-use efficiency, and nitrogen management," *AMBIO A. J. Human Environ.*, vol. 31, no. 2, pp. 132–140, Mar. 2002.

[9] A. Leone, M. N. Ripa, V. Uricchio, J. Deák, and Z. Vargay, "Vulnerability and risk evaluation of agricultural nitrogen pollution for Hungary's main aquifer using DRASTIC and GLEAMS models," *J. Environ. Manage.*, vol. 90, no. 10, pp. 2969–2978, Jul. 2009.

[10] R. W. Howarth, "Coastal nitrogen pollution: A review of sources and trends globally and regionally," *Harmful Algae*, vol. 8, no. 1, pp. 14–20, Dec. 2008.

[11] B. L. Bodirsky *et al.*, "Reactive nitrogen requirements to feed the world in 2050 and potential to mitigate nitrogen pollution," *Nature Commun.*, vol. 5, no. 1, Dec. 2014, Art. no. 3858.

[12] W. R. Raun *et al.*, "Improving nitrogen use efficiency in cereal grain production with optical sensing and variable rate application," *Agron. J.*, vol. 94, no. 4, pp. 815–820, 2002.

[13] B. Basso, B. Dumont, D. Cammarano, A. Pezzuolo, F. Marinello, and L. Sartori, "Environmental and economic benefits of variable rate nitrogen fertilization in a nitrate vulnerable zone," *Sci. Total Environ.*, vol. 545/546, pp. 227–235, Mar. 2016.

[14] C. Cilia *et al.*, "Nitrogen status assessment for variable rate fertilization in maize through hyperspectral imagery," *Remote Sens.*, vol. 6, no. 7, pp. 6549–6565, Jul. 2014.

[15] N. R. Kitchen *et al.*, "Ground-based canopy reflectance sensing for variable-rate nitrogen corn fertilization," *Agron. J.*, vol. 102, no. 1, pp. 71–84, 2010.

[16] J. Sawyer *et al.*, "Concepts and rationale for regional nitrogen rate guidelines for corn," Iowa State Univ.-Univ. Extension, Ames, IA, USA, White Paper, 2006.

[17] G. W. Randall and J. A. Vetsch, "Corn production on a subsurface-drained mollisol as affected by fall versus spring application of nitrogen and nitrapyrin," *Agron. J.*, vol. 97, no. 2, pp. 472–478, 2005.

[18] G. Schnitkey and L. Gentry, "The economic advisability of lowering 2019 nitrogen application rates on corn," *Farmdoc Daily*, vol. 9, Mar. 2019, Art. no. 48.

[19] J. Camberato and B. Nielsen, "Nitrogen management guidelines for corn in Indiana," in *Applied Crop Research Update.*, West Lafayette, IN, USA: Dept. Agronomy, Purdue Univ., Mar. 2019.

[20] J. A. Vetsch and G. W. Randall, "Corn production as affected by nitrogen application timing and tillage," *Agron. J.*, vol. 96, no. 2, pp. 502–509, 2004.

[21] M. K. Abbasi, M. M. Tahir, A. Sadiq, M. Iqbal, and M. Zafar, "Yield and nitrogen use efficiency of rainfed maize response to splitting and nitrogen rates in Kashmir, Pakistan," *Agron. J.*, vol. 104, no. 2, pp. 448–457, 2012.

[22] S. M. Mueller, J. J. Camberato, C. Messina, J. Shanahan, H. Zhang, and T. J. Vyn, "Late-split nitrogen applications increased maize plant nitrogen recovery but not yield under moderate to high nitrogen rates," *Agron. J.*, vol. 109, no. 6, pp. 2689–2699, Sep. 2017.

[23] C. M. Pittelkow *et al.*, "Tile drainage nitrate losses and corn yield response to fall and spring nitrogen management," *J. Environ. Qual.*, vol. 46, no. 5, pp. 1057–1064, Jun. 2017.

[24] R. H. Fox, C. L. Walthall, J. S. Schepers, and W. R. Raun, "Crop monitoring technologies to assess nitrogen status," in *Nitrogen in Agricultural Systems*. Madison, WI, USA: Amer. Soc. Agronomy, Inc., 2008, pp. 647–674.

[25] Á. Maresma, M. Ariza, E. Martínez, J. Lloveras, and J. Martínez-Casasnovas, "Analysis of vegetation indices to determine nitrogen application and yield prediction in maize (Zea mays L.) from a standard UAV service," *Remote Sens.*, vol. 8, no. 12, Nov. 2016, Art. no. 973.

[26] T. Morier, A. N. Cambouris, and K. Chokmani, "In-season nitrogen status assessment and yield estimation using hyperspectral vegetation indices in a potato crop," *Agron. J.*, vol. 107, no. 4, pp. 1295–1309, Feb. 2015.

[27] D. W. Barker and J. E. Sawyer, "Using active canopy sensors to quantify corn nitrogen stress and nitrogen application rate," *Agron. J.*, vol. 102, no. 3, pp. 964–971, 2010.

[28] G. Pajares, "Overview and current status of remote sensing applications based on unmanned aerial vehicles (UAVs)," *Photogramm. Eng. Remote Sens.*, vol. 81, no. 4, pp. 281–330, Apr. 2015.

[29] S. Candiago *et al.*, "Evaluating multispectral images and vegetation indices for precision farming applications from UAV images," *Remote Sens.*, vol. 7, no. 4, pp. 4026–4047, Apr. 2015.

[30] A. B. Potgieter *et al.*, "Multi-spectral imaging from an unmanned aerial vehicle enables the assessment of seasonal leaf area dynamics of sorghum breeding lines," *Front. Plant Sci.*, vol. 8, pp. 1532–1543, Sep. 2017.

[31] L. J. Thompson *et al.*, "Model and sensor-based recommendation approaches for in-season nitrogen management in corn," *Agron. J.*, vol. 107, no. 6, pp. 2020–2030, Jun. 2015.

[32] A. A. Gitelson, A. Viña, T. J. Arkebauer, D. C. Rundquist, G. Keydan, and B. Leavitt, "Remote estimation of leaf area index and green leaf biomass in maize canopies," *Geophys. Res. Lett.*, vol. 30, no. 5, pp. 1248–1252, Mar. 2003.

[33] M. S. Torino, B. V. Ortiz, J. P. Fulton, K. S. Balkcom, and C. W. Wood, "Evaluation of vegetation indices for early assessment of corn status and yield potential in the Southeastern United States," *Agron. J.*, vol. 106, no. 4, pp. 1389–1401, 2014.

[34] J. Bendig *et al.*, "Estimating biomass of barley using crop surface models (CSMs) derived from UAV-based RGB imaging," *Remote Sens.*, vol. 6, no. 11, pp. 10395–10412, Oct. 2014.

[35] M. Zaman-Allah *et al.*, "Unmanned aerial platform-based multi-spectral imaging for field phenotyping of maize," *Plant Methods*, vol. 11, no. 1, pp. 35–45, Dec. 2015.

[36] R. Houborg and M. F. McCabe, "A cubesat enabled spatio-temporal enhancement method (CESTEM) utilizing planet, landsat and MODIS data," *Remote Sens. Environ.*, vol. 209, pp. 211–226, May 2018.

[37] M. Jain *et al.*, "Mapping smallholder wheat yields and sowing dates using micro-satellite data," *Remote Sens.*, vol. 8, no. 10, Oct. 2016, Art. no. 860.

[38] K. Woellert, P. Ehrenfreund, A. J. Ricco, and H. Hertzfeld, "Cubesats: Cost-effective science and technology platforms for emerging and developing nations," *Adv. Space Res.*, vol. 47, no. 4, pp. 663–684, Feb. 2011.

[39] *USDA—National Agricultural Statistics Service Homepage*, USDA, 2018. [Online]. Available: https://www.nass.usda.gov/. Accessed on: Dec. 28, 2018.

[40] M. H. Siebers *et al.*, "Simulated heat waves during maize reproductive stages alter reproductive growth but have no lasting effect when applied during vegetative stages," *Agric. Ecosyst. Environ.*, vol. 240, pp. 162–170, Mar. 2017.

[41] *RedEdge Camera Radiometric Calibration Model—Micasense Knowledge Base*, MicaSense, 2018. [Online]. Available: https://support.micasense.com/hc/en-us/articles/115000351194-Rededge-Camera-Radiometric-Calibration-Model. Accessed on: Nov. 28, 2018.

[42] Y. Luo, K. Guan, and J. Peng, "STAIR: A generic and fully-automated method to fuse multiple sources of optical satellite data to generate a high-resolution, daily and cloud-/gap-free surface reflectance product," *Remote Sens. Environ.*, vol. 214, pp. 87–99, Sep. 2018.

[43] D. A. Ruiz Diaz, J. A. Hawkins, J. E. Sawyer, and J. P. Lundvall, "Evaluation of in-season nitrogen management strategies for corn production," *Agron. J.*, vol. 100, no. 6, pp. 1711–1719, Nov. 2008.

[44] N. Z. Jovanovic and J. G. Annandale, "Measurement of radiant interception of crop canopies with the LAI-2000 plant canopy analyzer," *S. Afr. Tydskr. Plant Grond*, vol. 15, no. 1, pp. 6–13, 1998.

[45] P. B. Reich, M. B. Walters, and D. S. Ellsworth, "From tropics to tundra: Global convergence in plant functioning," *Proc. Nat. Acad. Sci. USA*, vol. 94, no. 25, pp. 13730–13734, 1997.

[46] J. Bragagnolo, T. Jorge Carneiro Amado, R. da Silveira Nicoloso, J. Jasper, J. Kunz, and T. De Gregori Teixeira, "Optical crop sensor for variable-rate nitrogen fertilization in corn: I—Plant nutrition and dry matter production," *Revista Brasileira de Ciência do Solo*, vol. 37, no. 5, pp. 1288–1298, 2013.

[47] P. A. Townsend, S. P. Serbin, E. L. Kruger, and J. A. Gamon, "Disentangling the contribution of biological and physical properties of leaves and canopies in imaging spectroscopy data," *Proc. Nat. Acad. Sci. USA*, vol. 110, no. 12, Mar. 2013, Art. no. E1074.

[48] J. A. Gamon, B. Somers, Z. Malenovsky, E. M. Middleton, U. Rascher, and M. E. Schaepman, "Assessing vegetation function with imaging spectroscopy," *Surv. Geophys.*, vol. 40, pp. 489–513, 2019.

[49] J. L. Gabriel, P. J. Zarco-Tejada, P. J. López-Herrera, E. Pérez-Martín, M. Alonso-Ayuso, and M. Quemada, "Airborne and ground level sensors for monitoring nitrogen status in a maize crop," *Biosyst. Eng.*, vol. 160, pp. 124–133, Aug. 2017.

[50] L. Winterhalter, B. Mistele, and U. Schmidhalter, "Assessing the vertical footprint of reflectance measurements to characterize nitrogen uptake and biomass distribution in maize canopies," *Field Crops Res.*, vol. 129, pp. 14–20, Apr. 2012.

[51] S. Jacquemoud, C. Bacour, H. Poilvé, and J. P. Frangi, "Comparison of four radiative transfer models to simulate plant canopies reflectance: Direct and inverse mode," *Remote Sens. Environ.*, vol. 74, no. 3, pp. 471–481, 2000.

[52] J. L. Widlowski *et al.*, "The fourth phase of the radiative transfer model intercomparison (RAMI) exercise: Actual canopy scenarios and conformity testing," *Remote Sens. Environ.*, vol. 169, pp. 418–437, Nov. 2015.

[53] Z. Jin, R. Prasad, J. Shriver, and Q. Zhuang, "Crop model- and satellite imagery-based recommendation tool for variable rate N fertilizer application for the US Corn system," *Precis. Agric.*, vol. 18, no. 5, pp. 779–800, Oct. 2017.

[54] Y. Zeng, S. Jin, Q. Wu, and F. Gao, "Network-connected UAV communications," *China Commun.*, vol. 15, no. 5, pp. iii–v, May 2018.

[55] M. Campion, P. Ranganathan, and S. Faruque, "A review and future directions of UAV swarm communication architectures," in *Proc. IEEE Int. Conf. Electro/Inf. Technol.*, 2018, pp. 0903–0908.

[56] A. Poghosyan and A. Golkar, "CubeSat evolution: Analyzing CubeSat capabilities for conducting science missions," *Prog. Aerosp. Sci.*, vol. 88, pp. 59–83, Jan. 2017.

[57] M. Diacono, P. Rubino, and F. Montemurro, "Precision nitrogen management of wheat: A review," *Agron. Sustain. Dev.*, vol. 33, no. 1, pp. 219–241, Jan. 2013.

[58] Y. Cai *et al.*, "A high-performance and in-season classification system of field-level crop types using time-series Landsat data and a machine learning approach," *Remote Sens. Environ.*, vol. 210, pp. 35–47, Jun. 2018.

[59] D. E. Clay, K.-I. Kim, J. Chang, S. A. Clay, and K. Dalsted, "Characterizing water and nitrogen stress in corn using remote sensing," *Agron. J.*, vol. 98, no. 3, pp. 579–587, 2006.

Yaping Cai (S'19) received the B.A. degree in geography information system and the M.S. degree in photogrammetry and remote sensing from Peking University, Beijing, China, in 2011 and 2014, respectively. He is currently working toward the Ph.D. degree majored in geography and geographic information science at the University of Illinois at Urbana-Champaign, Urbana, IL, USA.

His current research interests include crop-type classification, crop yield prediction, and crop stress detection using multisource remote sensing data.

Kaiyu Guan received the B.A. degree in geography and geoinformatics from Nanjing University, Nanjing, China, in 2008, and the M.A. and Ph.D. degrees in water resources and environmental engineering from Princeton University, Princeton, NJ, USA, in 2010 and 2013, respectively.

From 2013 to 2015, he was a Postdoctoral Scholar with the Center of the Food Security and the Environment, Stanford University. From 2015 to 2016, he was a Quantitative Scientist with the Climate Corporation. Since 2016, he has been an Assistant Professor in ecohydrology and remote sensing with the Department of Natural Resources and Environmental Sciences, College of Agricultural, Consumer and Environmental Sciences, University of Illinois at Urbana Champaign, Champaign, IL, USA, where he is currently a Blue Waters Professor with the National Center for Supercomputing Applications. He is also a NASA New Investigator and leads multiple federal and state-level projects funded by NASA, USDA, etc. His research interests include using satellite data, computational models, field work, and machine learning approaches to address how climate and human practices affect crop productivity, water resource availability, and ecosystem functioning. He has keen interests in applying his knowledge and skills in solving real-life problems, such as large-scale crop monitoring and forecasting, water management and sustainability, and global food security.

Emerson Nafziger received the B.A. degree from Ohio State University, Columbus, OH, USA, in 1973, the M.S. degree from Purdue University, West Lafayette, IN, USA, in 1975, and the Ph.D. degree from the University of Illinois at Urbana-Champaign, Urbana, IL, USA, in 1982, all in agronomy.

He has been a Professor of crop sciences with the University of Illinois at Urbana-Champaign since 1993. He turns agronomic data collected from research throughout Illinois into tools that help producers better manage crops by predicting responses to crop inputs. He created a data-driven nitrogen rate calculator, an online resource that assists producers in improving nitrogen management for corn in most of the largest corn-producing states. His research interests include measuring the effect of crop rotation on response of corn to N fertilizer, cropping sequence and practices as they affect crop yield and yield stability, planting date and plant population effects on corn yield, simulated hail effects on corn, micronutrient and seed inoculant effects on corn and soybeans, variety testing, nitrogen and hybrid interactions, new N rate guidelines and on-farm corn N rate trials, and weed management in corn and soybeans.

Girish Chowdhary (M'13) received the Ph.D. degree from the Georgia Institute of Technology (Georgia Tech), Atlanta, GA, USA, in 2010.

He was a Research Engineer with the Institute for Flight Systems Technology, German Aerospace Center, Braunschweig, Germany. He was with Oklahoma State University–Stillwater, Stillwater, OK, USA, until 2016. He has postdoctoral experience with the Laboratory for Information and Decision Systems, Massachusetts Institute of Technology, Cambridge, MA, USA, and the School of Aerospace Engineering, Georgia Tech. He is currently an Assistant Professor with the Agriculture and Bioengineering School and the Aerospace Engineering School, University of Illinois at Urbana-Champaign, Champaign, IL, USA. His current research interests include theoretical foundations and practical algorithms for autonomous decision making and machine learning for complex cyberphysical systems that vary with space and time.
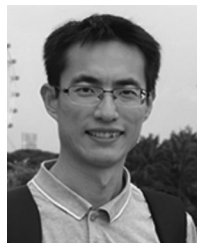
Dr. Chowdhary is a Member of the American Institute of Aeronautics and Astronautics, the IEEE Control Systems Society, and the Association for Unmanned Vehicle Systems International.

Bin Peng received the B.S. degree in geography from Nanjing University, Nanjing, China, in 2011, and the Ph.D. degree from the University of Chinese Academy of Sciences, Beijing, China, in 2016.

He is currently a Postdoctoral Research Fellow with the University of Illinois at Urbana-Champaign, Urbana, IL, USA. His current research interests include investigating land–atmosphere interactions, food-energy-water nexus through land surface modeling, hydrological modeling, crop modeling, remote sensing, and data assimilation approaches.

Dr. Peng has been a member of the International Association of Hydrological Sciences since 2012 and a member of the American Geophysical Union since 2016.

Zhenong Jin received the B.S. degree in ecology from Peking University, Beijing, China, in 2011, and the Ph.D. degree in earth and atmospheric science from Purdue University, West Lafayette, IN, USA, in 2016.

From 2016 to 2018, he was a Postdoctoral Scholar with the Center of the Food Security and the Environment, Stanford University. From 2018 to 2019, he was a Lead Crop Scientist with the Atlas AI P.B.C. Since 2019, he has been an Assistant Professor with the Department of Bioproducts and Biosystems Engineering and Data Analytics for Precision Agriculture. His research interests include mapping agriculture features using high-resolution satellite imagery, forecasting crop yields for a range of applications, integrating crop models with remote sensing for precision nitrogen management, and understanding the impacts of climate change on agroecosystem.

Shaowen Wang received the B.S. degree in computer engineering from Tianjin University, Tianjin, China, in 1995, the M.S. degree in geography from Peking University, Beijing, China, in 1998, and the M.S. degree in computer science and the Ph.D. degree in geography from the University of Iowa, Iowa City, IA, USA, in 2002 and 2004, respectively.

He is a Professor of geography and GIScience with the University of Illinois at Urbana-Champaign (UIUC), Champaign, IL, USA, where he is named a Centennial Scholar. He is also an Associate Director of the National Center for Supercomputing Applications for CyberGIS, and Founding Director of UIUC's CyberGIS Center for Advanced Digital and Spatial Studies. He is the Principal Investigator of several multi-institution National Science Foundation (NSF) projects for advancing cyberGIS and related scientific problem solving. He has authored many peer-reviewed papers including more than 20 journals.

Dr. Wang is currently serving as the President-Elect of the University Consortium for Geographic Information Science, and as a member of the U.S. National Research Council's Board on Earth Sciences and Resources. He was the recipient of NSF CAREER Award.

Sibo Wang received the B.S. degree in computer science and astronomy in 2018 from the University of Illinois at Urbana-Champaign, Urbana, IL, USA, where he is currently a graduate student with the Department of Natural Resources and Environmental Sciences.

His research interests include large-scale interoperable satellite data preparation in supercomputing environments and applying modern machine learning techniques to crop modeling.